JOURNAL OF TISSUE ENGINEERING AND REGENERATIVE MEDICINE
J Tissue Eng Regen Med 2018; **12**: e747–e759.
Published online 7 May 2017 in Wiley Online Library (wileyonlinelibrary.com) **DOI:** 10.1002/term.2365

RESEARCH ARTICLE

Antibacterial-nanocomposite bone filler based on silver nanoparticles and polysaccharides

Davide Porrelli[1,2]*, Andrea Travan[2], Gianluca Turco[1], Matteo Crosera[3], Massimiliano Borgogna[2], Ivan Donati[2], Sergio Paoletti[2], Gianpiero Adami[3] and Eleonora Marsich[1]
[1]*Department of Medicine, Surgery and Health Sciences, University of Trieste, Trieste, Italy*
[2]*Department of Life Sciences, University of Trieste, Trieste, Italy*
[3]*Department Chemical and Pharmaceutical Science, University of Trieste, Trieste, Italy*

Abstract

Injectable bone fillers represent an attractive strategy for the treatment of bone defects. These injectable materials should be biocompatible, capable of supporting cell growth and possibly able to exert antibacterial effects. In this work, nanocomposite microbeads based on alginate, chitlac, hydroxyapatite and silver nanoparticles were prepared and characterized. The dried microbeads displayed a rapid swelling in contact with simulated body fluid and maintained their integrity for more than 30 days. The evaluation of silver leakage from the microbeads showed that the antibacterial metal is slowly released in saline solution, with less than 6% of silver released after 1 week. Antibacterial tests proved that the microbeads displayed bactericidal effects toward *Staphylococcus aureus*, *Pseudomonas aeruginosa* and *Staphylococcus epidermidis*, and were also able to damage pre-formed bacterial biofilms. On the other hand, the microbeads did not exert any cytotoxic effect towards osteoblast-like cells. After characterization of the microbeads bioactivity, a possible means to embed them in a fluid medium was explored in order to obtain an injectable paste. Upon suspension of the particles in alginate solution or alginate/hyaluronic acid mixtures, a homogenous and time-stable paste was obtained. Mechanical tests enabled to quantify the extrusion forces from surgical syringes, pointing out the proper injectability of the material. This novel antibacterial bone filler appears as a promising material for the treatment of bone defects, in particular when possible infections could compromise the bone-healing process.

Received 11 March 2016; Revised 10 October 2016; Accepted 9 November 2016

Keywords **bone healing; injectable fillers; polysaccharides; antibacterial properties; silver nanoparticles**

1. Introduction

Injectable bone fillers represent an attractive strategy for the treatment of bone defects caused by traumatic injuries, cysts and pathologies characterized by an altered balance between bone tissue deposition and resorption (Lewis, 2011; Oliveira *et al.*, 2008; Page *et al.*, 2013). These materials can be employed when these defects are small and not treatable with bone auto- or allo-grafts, such as in case of scarcity of donors or in immunocompromised patients (Mauffrey *et al.*, 2015).

Novel injectable materials used as bone fillers should be biocompatible, support cell growth and possibly exert antibacterial effects in order to prevent infections (Kneser *et al.*, 2006; Page *et al.*, 2013). Moreover, upon injection, the material should tightly fit the defect cavity and remain *in situ* for the time required to form the new bone tissue (Ghanaati *et al.*, 2011; Kneser *et al.*, 2006).

Bone-filler materials can be prepared using various components, like synthetic or natural polymers, and bioceramic compounds (Alves Cardoso *et al.*, 2014; Bongio *et al.*, 2015; Nejadnik *et al.*, 2014; Page *et al.*, 2013; Sohrabi *et al.*, 2014; Tadier *et al.*, 2014). Among the bioceramic, hydroxyapatite (HAp) or β-tricalcium phosphate (β-TCP) have been widely employed owing to their osteoconductive properties (Bongio *et al.*, 2015; Kneser *et al.*, 2006).

Although these materials are effective in supporting bone tissue growth, the risk of periprosthetic infections remains a major threaten, especially in body districts with particular exposure to bacteria (e.g. mouth environment; Norowski and Bumgardner, 2009). These infections are a severe complication that can be as high as 5% of the total number of implants and, in the case of bone implants, can lead to tissue damage, implant failure or mortality (Campoccia *et al.*, 2006; Gristina, 1987). Despite that local delivery of antibiotics loaded on implantable biomaterials can be achieved (Wei *et al.*, 2012), the development of antibiotic resistances remains a severe problem (Campoccia *et al.*, 2006, 2010). To overcome this issue, the employment of alternative wide-spectrum antibacterial agents is sought (Lara *et al.*, 2011; Morones-Ramirez *et al.*, 2013); among them, silver ions and nanoparticles (nAg) have been successfully employed for the manufacturing of antibacterial bone implants (Goudouri *et al.*, 2014; Marsich *et al.*, 2013a; Reithofer *et al.*, 2014; Stojkovska *et al.*, 2014; Taglietti

*Correspondence to: Porrelli Davide, Department of Medicine, Surgery and Health Sciences, University of Trieste, Piazza dell'Ospitale 1, I-34129 Trieste, Italy. E-mail: dporrelli@units.it

et al., 2014; Travan *et al.*, 2009). Recently, a lactose-modified chitosan (Chitlac) has been employed for the synthesis of nAg, and the resulting system (Chitlac–nAg) was used to prepare antibacterial coatings (Marsich *et al.*, 2013b; Nganga *et al.*, 2013; Travan *et al.*, 2012). Moreover, the miscibility of Chitlac with alginate was previously exploited to prepare bioactive hydrogels in the form of scaffolds and microbeads, exploiting the gel-forming properties of alginate (Marsich *et al.*, 2008, 2013a; Travan *et al.*, 2009).

Given these premises, the scope of this work was to prepare and characterize microbeads based on alginate/Chitlac–nAg and HAp for bone tissue regeneration. Moreover, this study aimed at obtaining a preliminary evaluation of the possibility to obtain an injectable paste by embedding the microbeads in fluid medium, thus combining the osteoconductive and antibacterial properties of the components in an injectable bone-filler device.

2. Materials and methods

2.1. Materials

Sodium alginate samples isolated from *Laminaria hyperborea* were provided by FMC BioPolymer AS (Norway). The (viscosity average) relative molecular mass ('molecular weight', MW) was found to be approximately 120 000 as determined by capillary viscosimetry according to Vold *et al.* (2006). The composition of the alginate sample was determined by means of ^{1}H-NMR and resulted to be $F_G = 0.68$, $F_M = 1$, $F_G = 0.32$, $F_{GG} = 0.57$, $F_{GM+MG} = 0.22$, $F_{MM} = 0.21$, $N_{G>1} = 14$, where F_G and F_M denote the mole fraction of alginate monomers as α-L-guluronic acid (G) and β-D-mannuronic acid (M), respectively, F_{GG} indicates the fraction of G dimers, F_{MM} indicates the fraction of M dimers and F_{GM+MG} indicates the fraction of any mixed sequence of G and M (irrespective of sequence). $N_{G>1}$ is the number-average number ($-n_n$) of G monomer in homopolymeric sequences having $-n_n \geq 2$. Hyaluronic acid (HA150, MW 1 500 000) was provided by FMC BioPolymer AS (Norway). Highly deacetylated chitosan (residual acetylation degree approximately 16% as determined by means of ^{1}H-NMR) was purchased from Sigma-Aldrich (USA). The relative MW of chitosan, determined by intrinsic viscosity measurements, was found to be about 690 000 (Donati *et al.*, 2005). Chitlac (lactose-modified chitosan, CAS registry number 85941-43-1) was prepared according to the procedure reported elsewhere starting from highly deacetylated chitosan (Donati *et al.*, 2005; Yalpani and Hall, 1984). The composition of Chitlac was determined by means of ^{1}H-NMR and resulted to be: glucosamine residue 27%, N-acetylglucosamine 18% and 2-(lactit-1-yl)-glucosamine 55%. The calculated relative MW of Chitlac is about 1.5×10^6. Silver nitrate ($AgNO_3$), ascorbic acid ($C_6H_8O_6$), lactate dehydrogenase (LDH)-based TOX-7 kit, phosphate-buffered saline (PBS), Luria–Bertani (LB) broth, LB Agar and Brain Heart Infusion (BHI) were purchased from Sigma-Aldrich (USA). Trypsin/EDTA solutions, fetal bovine serum (FBS), penicillin streptomycin 100 ×, l-glutamine 100 × and Dulbecco's modified Eagle's medium (DMEM) were purchased from EuroClone (Milan, Italy). FilmTracer™ FM® 1-43 Green Biofilm Cell Stain and FilmTracer Live/Dead biofilm viability kit were purchased from Invitrogen (USA). All other chemicals were of analytical grade.

2.2. Synthesis of Chitlac–silver nanoparticles (Chitlac–nAg)

Silver nanoparticles (nAg) were obtained by reducing silver ions with ascorbic acid in Chitlac solution. Freeze-dried Chitlac was dissolved in deionized water to obtain a 4 g/l solution. Silver nitrate ($AgNO_3$) was added to Chitlac at a final concentration of 1 mM; then, ascorbic acid was added at a final concentration of 0.5 mM. The solution was kept for 4 h at room temperature in darkness and then stored at 4 °C.

2.3. Preparation of microbeads

Microbeads were prepared following a well-defined protocol previously reported by some of the authors (Marsich *et al.*, 2008; Travan *et al.*, 2009). Two types of microbeads have been prepared and tested: microbeads with silver nanoparticles (nAg–MB) and without silver nanoparticles (MB); both microbeads contained alginate, Chitlac and HAp. The MB have been prepared from an aqueous mixture composed by alginate (final concentration, 20 g/l), HAp (final concentration, 3% *w/V*) and Chitlac (final concentration, 2% g/l). In order to achieve a good miscibility of alginate and Chitlac, NaCl (final concentration 0.15 M) and HEPES (final concentration 0.01 M, pH 7.4) have been added to the mixture. The nAg–MB were prepared with the same procedure of the MB, employing Chitlac–nAg instead of Chitlac, as detailed in Section 2.2, at the final concentration of 2 g/l.

Microbeads without nAg and nAg–MB were obtained by dripping the mixed polymeric solutions into a gelling solution (aqueous 0.05 M $CaCl_2$). The droplet size was controlled by use of a high-voltage electrostatic bead generator (7.5 kV, 162 ml/h, steel needle with 0.7 mm outer diameter, 1 cm distance from the needle to the gelling solution), according to a procedure previously described (Travan *et al.*, 2009). The gel microbeads obtained were stirred for 30 min in the gelling solution and washed three times in deionized water.

Then, in order to obtain a material that could be easily handled and sterilized, microbeads were dried under air flux. Microbeads were sterilized for 1 h, under UV irradiation, before use in the biological tests.

2.4. Evaluation of total silver content and silver release

The total amount of silver in the nAg–MB and released from nAg–MB, soaked in saline or in deionized water, was determined by inductively coupled plasma-optical emission spectroscopy (ICP-OES) using an Optima 8000 ICP-OES Spectrometer (PerkinElmer, USA). The analyses were conducted using a calibration curve obtained by dilution (range: 0–10 mg/l) of a silver standard solution (10 015 μg/ml) for ICP-OES analyses (Sigma-Aldrich, USA). The limit of detection at the operative wavelength of 328.068 was 0.016 mg/l. The precision of the measurements as relative standard deviation for the analysis was always less than 5%.

The total amount of silver in the nAg–MB (ng Ag/mg beads) was measured upon treatment with concentrated H_2SO_4 and solubilization with concentrated HNO_3. About 9 mg of microbeads was degraded in 60 μl of H_2SO_4, than the volume was adjusted to 1.2 ml with HNO_3 to ensure the solubilization of silver precipitates. At the end, the volume was adjusted to 5 ml with deionized water. The average amount of silver was calculated as the mean of silver quantity measured in three samples.

For the quantification of silver released from the nAg–MB, about 50 mg of sample was incubated, in agitation, with a volume ratio solution/microbeads of 10. Every 24 h, supernatants from the microbeads suspensions were collected and analysed, and fresh solution was added to the microbeads. After the last solution change, the microbeads were washed with filtered deionized water to recover all the precipitated silver salts; the solution was then filtered (0.22 μm) and collected.

2.5. Scanning electron microscopy (SEM)

The air-dried microbeads were mounted on aluminium stubs covered with two-sides conductive carbon adhesive tape. Next, the samples were sputtered with gold (Sputter Coater K550X, Emitech, Quorum Technologies, UK) and immediately analysed by means of a SEM (Quanta250 SEM, FEI, Oregon, USA) operated in secondary electron detection mode. The working distance was adjusted in order to obtain the suitable magnification; the accelerating voltage was set to 30 kV.

2.6. Microbeads swelling and stability

The swelling and stability of microbeads were measured as the average diameter variation upon immersion in simulated body fluid (SBF) prepared as reported by Kokubo *et al.* (1990). Each test was performed in triplicate on a known number of beads (70–100 range). The diameter variation of the microbeads was measured by collecting the images with a Pentax K100D camera mounted on an optical microscope (Olympus CK 2, Tokyo, Japan); the diameter of beads population was measured by means of an image analysis software (ImageJ, USA). The microbeads were analysed every 2 days from the beginning of the swelling experiment. From day 15, diameters were recorded every week. The soaking solution was changed every 2 days.

2.7. Preparation of the injectable bone filler (paste)

The microbeads (30% *w*/w) were dispersed in the polysaccharide solution and transferred into syringes (1 ml, nozzle diameter 2 mm; Chemil, Italia). The solution was composed either by alginate (4% *w/V*) or by alginate (3% *w/V*) plus hyaluronic acid (1% *w/V*).

2.8. Injectability tests

The injectability tests were performed by applying an axial compression load to the syringe plunger by means of a Universal Testing Machine (Mecmesin MultiTest 2.5-I) coupled with a 100 N load cell. A compression rate of 15 mm/min was applied along 50 mm of plunger displacement, recording the load applied. For each formulation, five replicates have been used; the average load in the plateau region was measured and standard deviations calculated.

2.9. Antibacterial tests

The antibacterial activity of nAg–MB was evaluated using strains of *Staphylococcus epidermidis* (ATCC® 12228™), *Staphylococcus aureus* (ATCC® 25923™) and *Pseudomonas aeruginosa* (ATCC® 27853™), and using MB as a control.

2.10. Growth inhibition assay

Bacterial suspensions were prepared by adding 20 μl of bacteria, preserved in glycerol, to 5 ml of LB broth. The obtained suspensions were incubated overnight at 37 °C. After 24 h, 500 μl of bacterial suspension was diluted in 10 mL of broth and grown up for 90 min at 37 °C in order to restore an exponential growth phase. Bacterial concentration was measured by means of optical density at 600 nm. The bacterial suspension was then diluted in 10% (*v*/v) LB broth in PBS to obtain a final concentration of 10^6 bacteria/ml; 1 ml of bacterial suspension was added to each microbeads sample (50 mg). *S. aureus* and *P. aeruginosa* were incubated at 37 °C for 4 h, *S. epidermidis* for 24 h. Tests were carried out in shaking condition (140 r.p.m.). At the end of the incubation, bacterial suspension was collected and serially diluted in PBS (from 10^{-1} to 10^{-5}), and 25 μl of each suspension was plated on LB agar. After overnight incubation at 37 °C, the colony-forming units (CFUs) were counted. Outcomes were compared with a suspension of bacteria grown in liquid medium as control. Data are reported as the mean of three independent determinations.

2.11. Biofilm formation

Bacterial suspensions of *S. aureus* and *P. aeruginosa* were prepared by adding 20 μl of bacteria, preserved in glycerol, to 5 ml of BHI broth enriched with 3% *w/v* sucrose. The obtained suspensions were incubated overnight at 37 °C. After 24 h, bacteria were diluted 1:100 in the same broth and plated (200 μl/well) into 96-well plates. For confocal laser-scanning microscopy (CLSM) analyses, bacteria were plated on sterile 13-mm tissue culture coverslips (Sarstedt, USA) placed on the bottom of culture plate wells. Plates were incubated at 37 °C for 24 h allowing biofilm formation. After 24 h, broth was removed, and formed biofilm was carefully rinsed with 100 μl of sterile PBS in order to remove non-adherent cells; 200 μl of 10% LB in PBS was then added to each well and microbeads were deposited on the bacterial layer. Biofilms treated with microbeads were then incubated at 37 °C for 4 h; then the viability of the biomass was assessed, as described in the following paragraph.

2.12. Viable biomass assessment

The viable biomass assessment was performed staining the biofilm with the FilmTracer™ FM® 1-43 Green Biofilm Cell Stain. The staining solution was prepared by diluting 10 μl of stock solution into 990 μl of dimethylsulphoxide, followed by diluting 100 μl into 0.9 ml of filter-sterilized water. After the biofilm incubation period, microbeads and medium were gently removed from the plates, and each well was carefully rinsed with filter-sterilized deionized water, in order to remove non-adherent cells; 20 μl of staining solution was placed into each well and the plates were incubated for 30 min under lightproof conditions at room temperature. After the incubation period, each well was washed with filter-sterilized deionized water; then 80 μl of deionized water was added and the fluorescence was read with a spectrofluorimeter (λ_{exc} 485 nm, λ_{em} 520 nm, FLUOstar Omega, BMG LABTECH, Germany). Outcomes were expressed as fluorescence units.

2.13. CLSM

Confocal laser-scanning microscopy studies were addressed at detecting viability/death of bacteria grown in the biofilm community. FilmTracer Live/Dead biofilm viability kit was used. Dead cells were stained by propidium iodide (red fluorescence: λ_{exc} 514 nm; λ_{em} 590 nm), whereas live cells were stained by SYTO® 9 (green fluorescence: λ_{exc} 488 nm; λ_{em} 515 nm). Staining was performed on biofilms grown on coverslips as described above, according to the manufacturer's protocol. Images were acquired on a Nikon Eclipse C1si CLSM with a Nikon Plan Fluor 20 × as objective. Resulting stacks of images were analysed using ImageJ software.

2.14. Osteoblast cell culture

Osteosarcoma MG-63 (ATCC® CRL-1427) human cell line was cultured in DMEM high-glucose (Euro-Clone, Italy), 10% heat-inactivated FBS (Sigma Aldrich Chemical, USA), 100 U/ml penicillin, 100 μg/ml streptomycin and 2 mM L-glutamine in a humidified atmosphere of 5% CO_2 at 37 °C. Cells were passaged at 80–90% of confluence and medium was changed every 2 days. For the experimental procedures, cells at the fourth/fifth passage were used.

2.15. Cytotoxicity tests

In vitro cytotoxicity of nAg–MB was evaluated by using LDH cytotoxicity assay (SIGMA TOX-7LDH assay), and using MB as a control. UV-sterilized microbeads were placed in DMEM, inactivated FBS 10%, penicillin 100 U/ml, streptomycin 100 μg/ml and L-glutamine 2 mM for 24 h. After 24 h of incubation, the cytotoxicity test was performed by direct contact of the cells with the swollen microbeads (20 mg per well). Cells were seeded into 24-well plates (30 000 cells per well) and incubated for 24 h before the cytotoxicity test. After the first day, the medium was changed and the cells were incubated for 24 and 72 h with microbeads. After 24 and 72 h, the medium was collected and the test was performed following the manufacturer's protocol. The experiments were performed in triplicate. The absorbance was measured at 490 nm and 690 nm, with a Tecan Nano Quant Infinite M200 Pro plate reader. The cytotoxicity was calculated using the following equation:

$$\%LDH\ release = 100 \times \frac{(A_{490} - A_{690} treated\ cells) - (A_{490} - A_{690} medium)}{(A_{490} - A_{690} cell\ lysate) - (A_{490} - A_{690} medium)}$$

normalizing the values for the total LDH of the control cell lysate. Polystyrene (PS) was used as a negative control; zinc-embedded polyurethane (PU/Zn) membrane was used as positive control.

Moreover, at 72 h, before collection of the medium, images of cells were taken with a Pentax K100D camera mounted on an optical microscope (Olympus CK 2, Tokyo, Japan).

2.16. Statistical analyses

Statistical analyses were performed by means of SPSS Statistics 21 (IBM SPSS Statistics; SPSS, Chicago, IL, USA). Data of the bacterial growth inhibition satisfied both the normality (Kolmogorov–Smirnov test) and equality variance (Levene test) assumptions allowing therefore to use a *t*-test. Both the data for the intensity of fluorescence of the biofilm and the LDH release were not normally distributed according to Levene's test, Kruskal–Wallis and Mann–Whitney non-parametric tests were therefore used. Statistical significance was pre-set at $\alpha = 0.05$.

DOI: 10.1002/term

3. Results and discussion

3.1. Microbeads preparation

This work aimed at the preparation and characterization of nanocomposite microbeads to be used as bioactive bone fillers. Microbeads based on the mixture of the selected polysaccharides were prepared by exploiting the gel-forming properties of alginate: the hydrogel beads were prepared dropping the aqueous mixtures of the biopolymers into an aqueous solution of $CaCl_2$. In order to control the size of the beads, an electrostatic generator was used (Figure 1A). This technique is widely used in the literature for the preparation of biocompatible polysaccharide microbeads (Morch *et al.*, 2006; Travan *et al.*, 2009) and can be used for the encapsulation of cells within alginate gel matrices (Marsich *et al.*, 2008).

To further implement the bioactivity of the beads, the lactose-modified chitosan (Chitlac) was added to the polymer mixture. Previous studies by some of the authors have demonstrated that Chitlac possesses bioactive properties: in Marsich *et al.* (2008) and Donati *et al.* (2005), it was reported that Chitlac is able to stimulate the growth and proliferation of chondrocytes, and the production of chondro-specific glycosaminoglycans and collagen. Chitlac has also been used for the preparation of bioactive coatings for methacrylic thermosets (Travan *et al.*, 2012) and alginate scaffolds (Marsich *et al.*, 2013a), showing bioactive properties in terms of increased osteoblasts proliferation, alkaline phosphatase activity and bone–implant contact in the case of chitlac-coated thermosets (Marsich *et al.*, 2013b).

Moreover, to confer antibacterial properties to the materials, silver nanoparticles have been *in situ* synthesized within Chitlac solutions before being added to alginate solutions. As reported by Travan *et al.* (2009), silver nanoparticles synthesized in Chitlac display high stability and homogeneous dimensions, and are able to exert antibacterial effects without being toxic towards eukaryotic cells.

In the present study, the method adopted for the preparation of the microbeads enabled to obtain hydrogel microbeads with a narrow size distribution and an average size of 990 ± 60 μm, as determined by optical microscopy imaging; Figure 1B–D points out that the size distribution was similar for microbeads with (nAg–MB) or without (MB) silver nanoparticles.

The concentrations of alginate and HAp were optimized in order to reach a compromise between the maximization of the concentration of the osteoconductive component and the formation of a stable alginate mesh in the microbeads (Turco *et al.*, 2009).

In order to obtain the dried composite powder required for the sterilization of the material and the preparation of the injectable filler, the hydrogel beads were dehydrated by air flux, thus obtaining the dried composite particles. The dried particles were analysed by SEM in order to evaluate size and morphology; as expected, drying the hydrogel microbeads led to a significant reduction of their dimensions (MB: 250 ± 40 μm; nAg–MB: 270 ± 40 μm). These values are in the range commonly employed for the preparation of composite bone fillers based on HAp or β-TCP (Suzuki *et al.*, 2014; Tadier *et al.*, 2014).

The SEM analysis enabled also to highlight how the bead surfaces are roughened by the presence of HAp crystals that protrude from both MB and nAg–MB particles (Figure 2B and D).

3.2. Swelling and stability

The swelling behaviour and stability were investigated by incubating the dried microbeads in SBF at 37 °C and replacing it at fixed days. SBF is widely used for the evaluation of the stability and the apatite-forming properties of biomaterials for bone tissue regeneration (Díez-Pascual and Díez-Vicente, 2015; Gervaso *et al.*, 2016; Tan *et al.*, 2010; Turco *et al.*, 2009). In this work, the stability evaluation was performed without the use of degradation enzymes as it is known that there are no

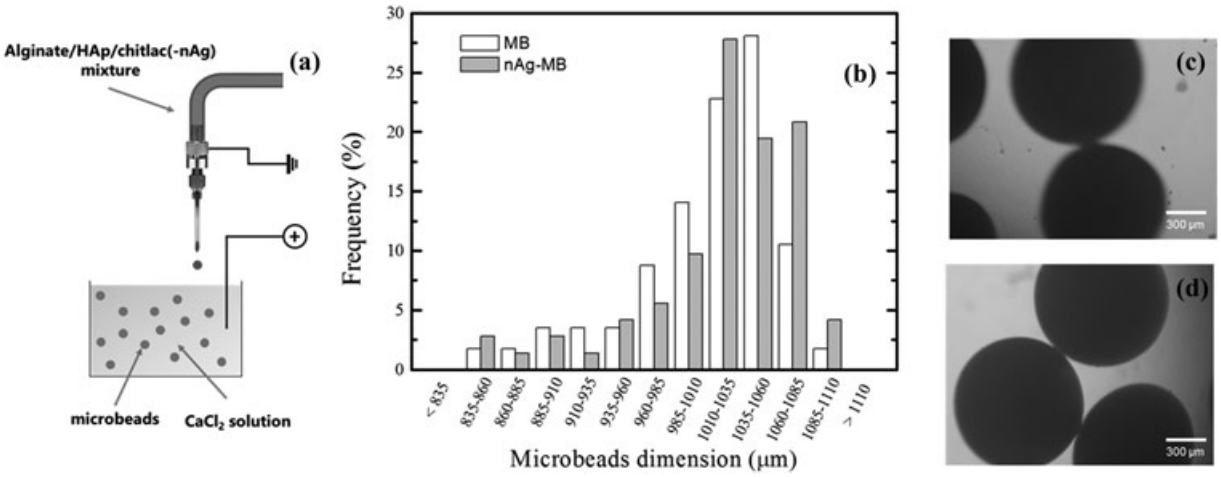

Figure 1. (A) Schematic representation of the preparation of the microbeads: the alginate/HAp/Chitlac (with or without nAg) solution is dropped in a $CaCl_2$ solution under the application of a voltage. (B) Dimension distribution of MB and nAg–MB. On the right, microbeads aspect: (C), MB. (D) nAg–MB

DOI: 10.1002/term

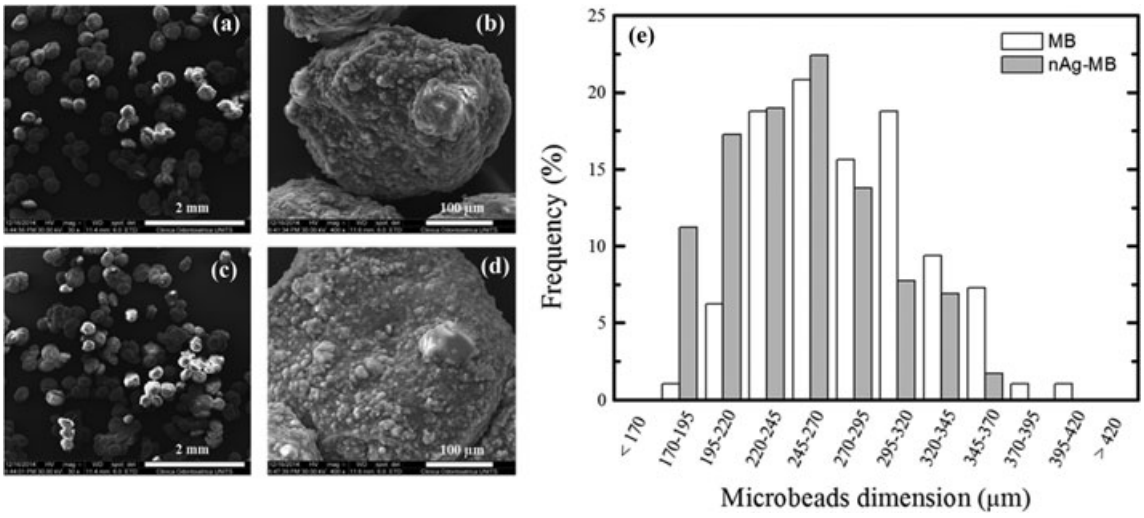

Figure 2. Scanning electron microscope (SEM) micrographs of MB (A, B) and nAg–MB (C, D). (E) Distribution of microbeads dimension: MB and nAg–MB

specific enzymes in mammalians for the degradation of alginate (Guarino *et al.*, 2015; Lee and Mooney, 2012). Moreover, it has been demonstrated that the enzyme lysozyme has only a minor effect on chitosan, and that this effect becomes even smaller when chitosan is functionalized with lactose (Diolosá *et al.*, 2014).

The size variation of the microbeads soaked in SBF over time is reported in Figure 3A: the data show how the microbeads underwent a considerable swelling leading to an increase of their dimension, owing to the presence of the hydrophilic polysaccharides. The microbeads rapidly (approximately 2 days) reached a swelling equilibrium, with an increase of diameter and volume that was, respectively, 3.5-fold and 43-fold compared with the initial values. The swelling rate of MB and nAg–MB was similar (Figure 3A) and did not affect the morphology of the microbeads (Figure 3B,C).

The experiment went on for 31 days, pointing out the excellent morphological stability of the microbeads, which did not show any significant degradation in physiological-like conditions. These data confirm the stability of biomaterials based on alginate hydrogels containing HAp, as already observed in the case of tridimensional scaffolds for bone tissue regeneration (Porrelli *et al.*, 2015; Turco *et al.*, 2009).

Considering the final application (the preparation of an injectable system), the swelling and degradation behaviour found represents a positive feature of the material. This feature enables the injectable filler to adapt to the bone defect and remain firmly *in situ* for several weeks, thus assisting the natural bone regrowth process. In fact, the prolonged stability of an injectable material is a key factor in the regeneration of the bone tissue (von Doernberg *et al.*, 2006; Ghanaati *et al.*, 2011;

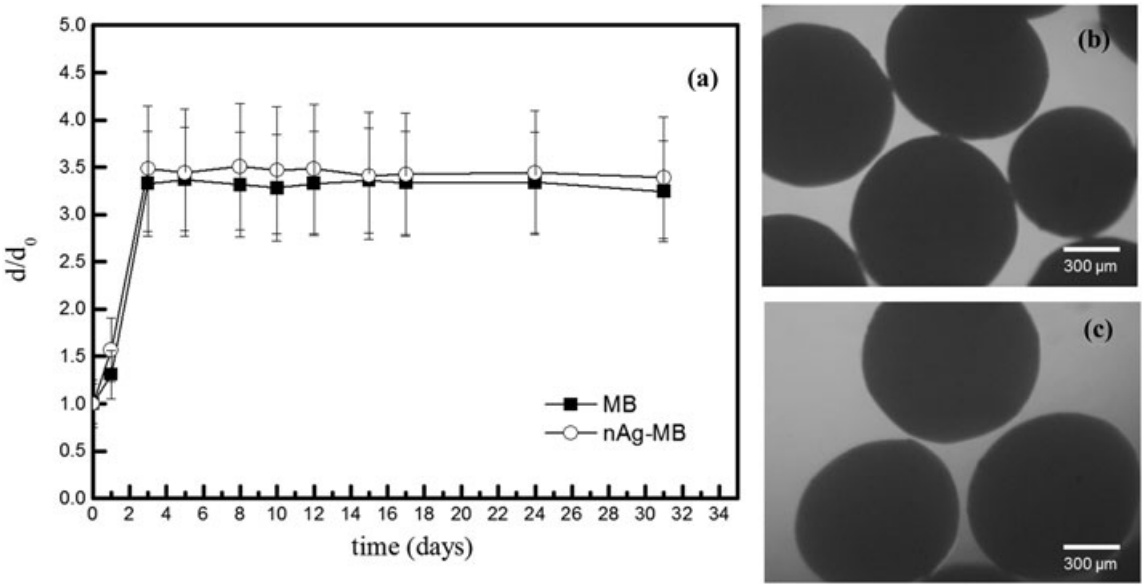

Figure 3. (A) Diameter changes during the swelling experiment. On the right, microbeads aspect after 32 days of experiment. (B), MB. (C) nAg–MB

DOI: 10.1002/term

Grynpas *et al.*, 2002), as new bone tissue formation requires several weeks (Urist, 1965).

3.3. Silver release from nAg–MB

The amount of silver contained in the nAg–MB has been quantified by means of ICP-OES; the analysis revealed that 1 mg of microbeads contains 0.978 ± 0.146 μg of silver (data averaged on three samples).

The silver release from the nAg–MB has been measured soaking the microbeads in deionized water and in saline solution (NaCl 0.15 M); in order to put the particles in contact with abundant liquid, the ratio between the volume of water/solution and the volume of microbeads was 10. To mimic real conditions, the solutions were changed every 24 h and the microbeads were subjected to mechanical agitation. The silver released from the microbeads over time was reported both as the percentage of silver released each day (Figure 4A) or as the cumulative release (Figure 4B).

The data point out that for both water and saline solution the silver released upon daily shifts is typically lower than 1%, while after 7 days the cumulative silver release was 5.69 ± 0.95% in saline solution and 0.36 ± 0.12% in water. The higher release in saline is explainable considering that the presence of ions can accelerate the swelling of the polymer mesh, which increases the exposure of silver nanoparticles to the environment. Moreover, it is known that the dissolution of silver nanoparticles and the release of silver ions are influenced by ionic strength and the chloride concentration of the solution (Chambers *et al.*, 2014). However, in both cases, the silver release was very low as only 0.56 ng per mg of bead has been released after 7 days, thus proving the structural stability of the polymer mesh.

Comparing the results of silver release and swelling behaviour of the microbeads, one could expect a burst release of silver in a timeframe compatible with the swelling of the microbeads (Figure 3); however, the results did not point out such behaviour. The absence of a burst release can be explained considering that in this system the silver nanoparticles are chemically stabilized by Chitlac, which in turn is closely embedded in the alginate matrix of microbeads.

The amount of silver released from nAg–MB is higher if compared with that of alginate/Chitlac–nAg hydrogels devoid of HAp reported by Travan *et al.* (2009); this result can be explained by the fact that the introduction of HAp can affect the formation of alginate egg-box, thus reducing the stability of the material. However, the silver released from nAg–MB is lower than that reported for tridimensional alginate/HAp scaffolds coated with Chitlac–nAg (Marsich *et al.*, 2013a), thus pointing out that silver release can be tuned by employing different methods of incorporation in the biomaterial.

Overall, the profile of the silver released from the nAg–MB appears particularly appealing for bone tissue engineering applications, as it ensures a long-term stability of the antibacterial agent, thus avoiding a burst release of metal ions that could potentially be toxic for the cells of the surrounding tissues. Moreover, the slow release of silver contributes to prolong the antibacterial effect of the nanoparticles, which is also related to the direct contact with bacterial cells (Travan *et al.*, 2009).

3.4. Antibacterial properties

The antibacterial properties of nAg–MB were assessed in terms of inhibition of bacterial growth and eradication of biofilms produced by three bacterial strains: *S. aureus*, *P. aeruginosa* and *S. epidermidis.* These strains have been selected because of their role in bone-related infections and their antibiotic-resistance mechanisms (Gottenbos *et al.*, 2000; Kilgus *et al.*, 2002; Moran *et al.*, 2010; Parvizi *et al.*, 2009; Toms *et al.*, 2006). The assays have been performed incubating the microbeads (nAg–MB or MB) in direct contact with bacteria for chosen times.

For *S. aureus* and *P. aeruginosa,* the growth inhibition assay was performed by incubating the bacterial suspension with the dried microbeads for 4 h, after which the CFUs were measured; in both cases, the nAg–MB induced a significant decrease of the CFU,

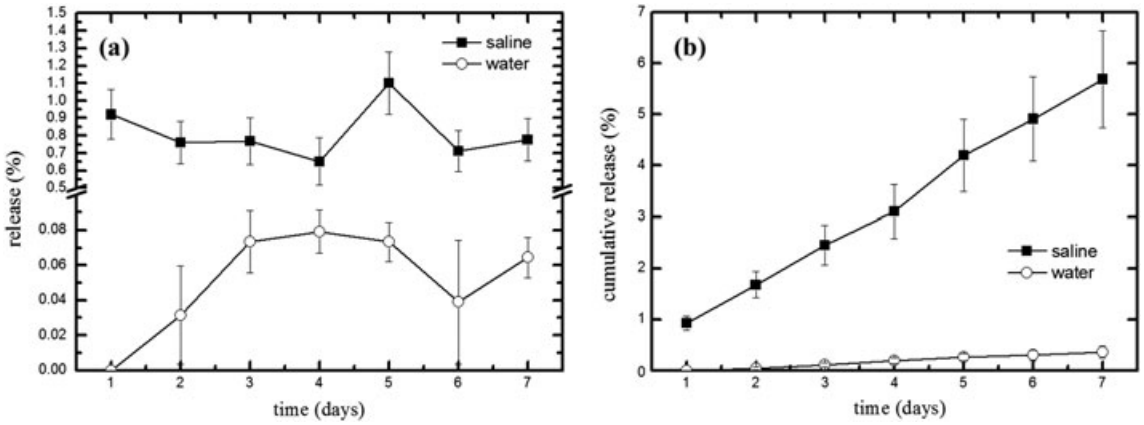

Figure 4. Silver released by the microbeads (nAg–MB) soaked in deionized water or in saline solution expressed as a percentage of the total silver contained: (A) release at given solution shift; (B) cumulative release. Data were averaged on three independent experiments

whose number was reduced by several orders of magnitude (Figure 5A,B).

In the case of *S. epidermidis*, no antibacterial effect was detected after 4 h of incubation (data not shown). For this reason, the incubation was prolonged to 24 h, which revealed to be a sufficient time for the nAg–MB to exert a bactericidal effect; in fact, a decrease of more than four orders of magnitude was found in the case of the silver-containing particles (Figure 5C). The observed higher resistance of *S. epidermidis* was in line with the results reported in a previous work by Marsich *et al.* (2013a).

Once the effectiveness of the silver-containing particles in inhibiting bacterial growth had been verified, a further test has been carried out to evaluate their effect towards pre-formed biofilms. This assay was performed on *S. aureus* and *P. aeruginosa* strains, as *S. epidermidis* does not produce a self-protecting biofilm. Bacterial biofilms were put in contact with the microbeads for 4 h and the bacteria viability was quantified using the Green Biofilm Cell Stain assay, which exploits the fluorescence intensity of the biomass as an indicator of viable bacteria within the biofilm. The results are reported in Figure 6. In the case of *S. aureus*, the nAg–MB displayed a strong anti-biofilm activity, as a 69% decrease of the fluorescence intensity was measured with respect to the control. In the case of *P. aeruginosa* the nAg–MB determined a 26% reduction of the biofilm fluorescence intensity; this milder effect could be ascribed to the high content of alginate in the *P. aeruginosa* biofilm, which represents a physical barrier towards antibacterial agents (Leid *et al.*, 2005).

The viability of bacteria within biofilms was also evaluated by the Live/Dead assay, which, by means of a fluorescence microscope, enables to distinguish between viable cells (green) and dead cells (orange-red); Figure 7 collects the images of the biofilms after 4 h of treatment with the particles, compared with untreated (control) biofilms.

In the case of *S. aureus*, the images clearly show the abundance of viable bacteria (green) for untreated (Figure 7A) and MB-treated biofilms (Figure 7B); at variance, the treatment withnAg–MB causes a clear inactivation of bacterial cells, appearing as red particles (Figure 7C). In the case of *P. aeruginosa,* the antibacterial effect of the nAg–MB can be inferred by the abundance of orange/red biomass (Figure 7G), at variance with control (Figure 7E) and MB-treated bacteria (Figure 7F). Thus, the Live/Dead results are in line with the results of the Green Biofilm Cell Stain assay, both pointing out the antibacterial effect of nAg–MB on pre-formed biofilms.

Overall, the assays performed confirm the antibacterial properties of nAg–MB, in concordance with the data previously reported for alginate-based hydrogels (Travan *et al.*, 2009) or scaffolds (Marsich *et al.*, 2013a) enriched with Chitlac–nAg.

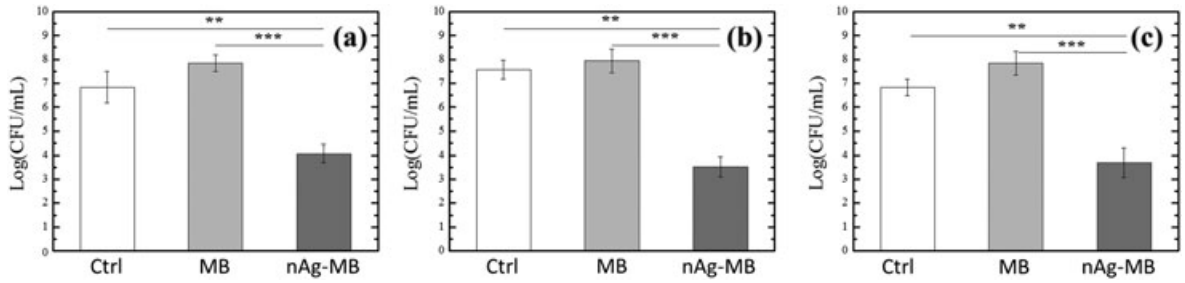

Figure 5. Growth inhibition assay of bacteria treated with microbeads (MB or nAg–MB), compared with the growth control (Ctrl). *Staphylococcus aureus* (A), *Pseudomonas aeruginosa* (B) were incubated for 4 h, while *Staphylococcus epidermidis* (C) was incubated for 24 h. Statistical differences were determined by means of Student's *t*-test. $^{**}P < 0.01$; $^{***}P < 0.001$

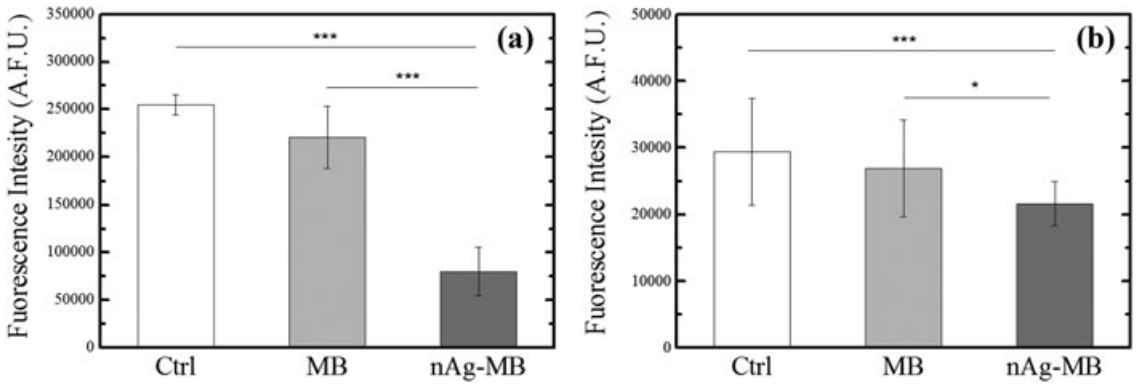

Figure 6. Effect of microbeads on biofilms of *Staphylococcus aureus* (A) and *Pseudomonas aeruginosa* (B) after 4 h of contact with the materials (Green Biofilm Cell Stain assay). Ctrl: untreated biofilm; MB: biofilm treated with MB particles; nAg–MB: biofilm treated with nAg–MB particles. Statistical significance was evaluated by Kruskal–Wallis and Mann–Whitney non-parametric tests. $^{*}P < 0.05$; $^{**}P < 0.01$; $^{***}P < 0.001$

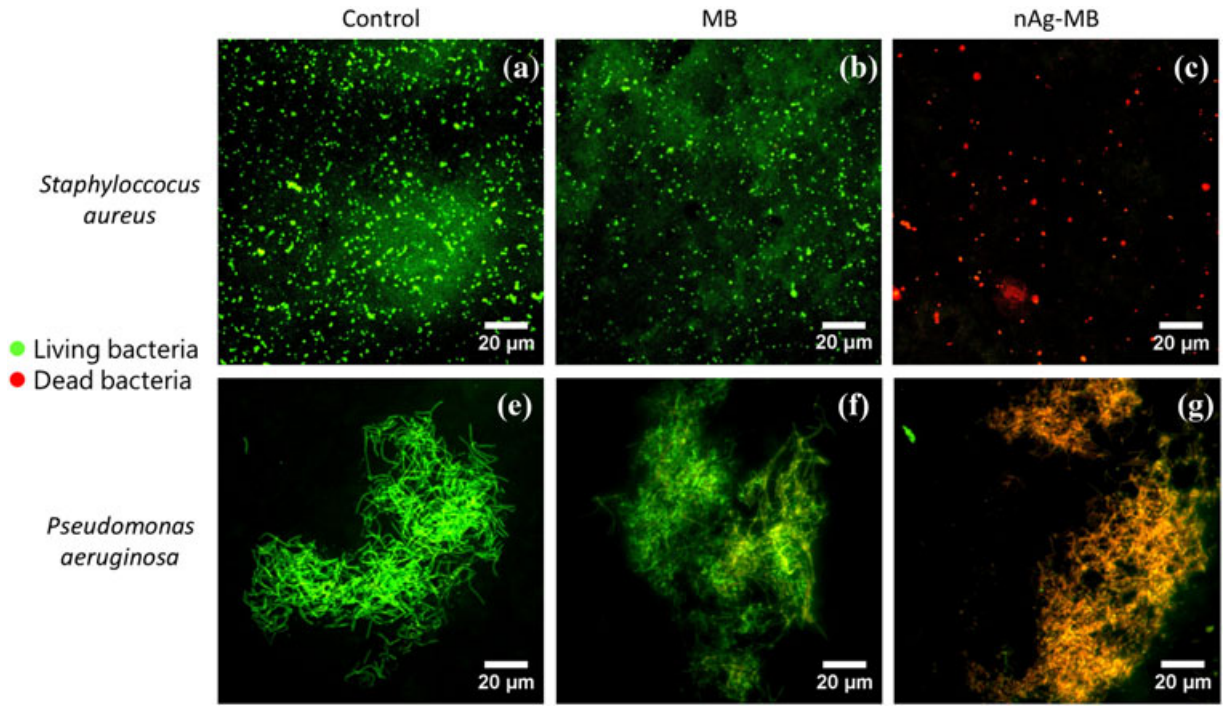

Figure 7. Effect of microbeads on biofilms of *Staphylococcus aureus* (A–C) and *Pseudomonas aeruginosa* (E–G) after 4 h of contact with the materials (Live/Dead assay). Control: untreated biofilm; MB: biofilm treated with MB particles; nAg–MB: biofilm treated with nAg–MB particles. For all images, green fluorescence (SYTO® 9) indicates live cells, whereas red fluorescence (propidium iodide) refers to dead ones

3.5. Cytotoxicity and viability

After studying the antibacterial activity of the microbeads, their effect towards eukaryotic cells was evaluated by the LDH assay, which enables to quantify the release of the LDH enzyme due to cellular damage; the assay has been carried out by putting an osteoblasts cell line (MG63) in direct contact with the cells with microbeads for 24 and 72 h (according to the ISO 10993-5 standard, 1999). Figure 8 shows the results of this cytotoxicity study as well as a qualitative evaluation of the morphology of the cells in contact with the materials.

The results of Figure 8A pointed out that both MB and nAg–MB particles were associated with low values ($< 15\%$) of LDH release, which remained significantly lower than the positive (cytotoxic) control (PU/Zn). These quantitative data were confirmed by the qualitative investigation of cell morphology (Figure 8B), which highlighted the healthy conditions of the cells proliferated on the multiwell floor in direct contact with both types of microbeads.

The data here-reported confirm the biocompatibility of silver nanoparticles stabilized within the Chitlac matrix and the suitability of Chitlac–nAg for the preparation of bioactive polysaccharide-based biomaterials, in line with previous approaches by some of the authors (Marsich *et al.*, 2013a; Travan *et al.*, 2009, 2012). The slight increase of cytotoxicity observed at 72 h can be due to

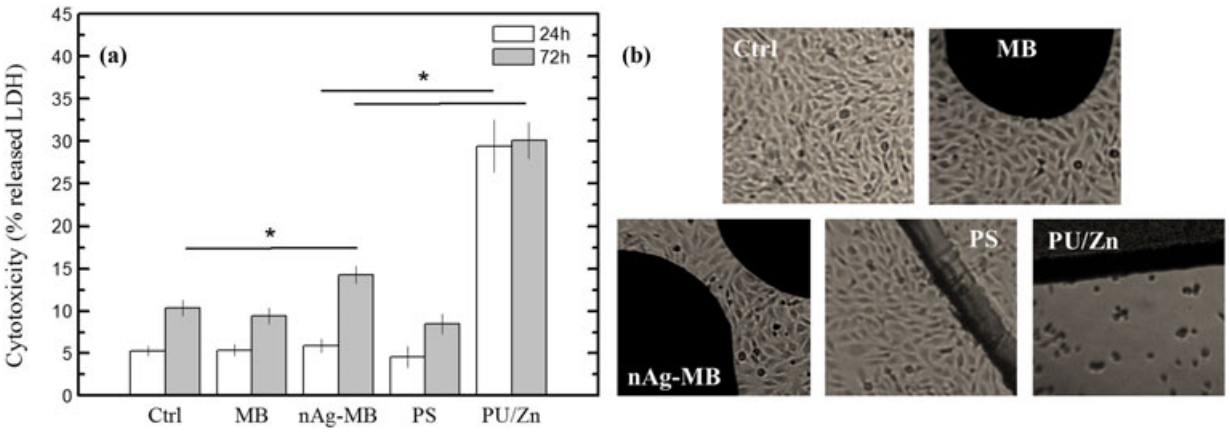

Figure 8. Evaluation of material cytotoxicity towards MG63 osteoblast-like cells. (A) Lactate dehydrogenase (LDH) assay after 24 h and 72 h on cells in direct contact with the materials. Ctrl: adhesion control on multiwall; MB: cells in contact with MB particles; nAg–MB: cells in contact with nAg–MB particles; PS: cells in contact with polystyrene membrane (negative control); PU/Zn: cells in contact with polyurethane/zinc membranes (positive control). Statistical differences were determined by means of Kruskal–Wallis and Mann–Whitney non-parametric tests. $^{*}P < 0.05$. (B) Microscopic image of the cells after 72 h

two different factors: (i) the accumulation of silver in the culture medium, which was not changed during the test according to the standardized protocol; (ii) the limited mimicking of the *in vivo* conditions in a cytotoxicity assay on 2D-cultured cells. These hypotheses are supported by Stojkovska *et al.* (2014), who reported a higher cytotoxicity of silver nanoparticles on 2D cultures of chondrocytes with respect to the 3D environment of perfused bioreactors. Moreover, according to the standards for the determination of the cytotoxicity of materials (accordingly to the ISO 10993-5 standard, 1999), the values of LDH released by the cells in contact with nAg–MB are significantly lower than the threshold considered as cytotoxic (30% of LDH released over the total content).

3.6. Injectability studies

As soon as the composite microbeads were characterized and their biological properties assessed, the material was employed for the preparation of an injectable system based on dried MB suspended in a suspending liquid medium. The latter was selected through a preliminary screening of polysaccharide solutions by evaluating the homogeneity and stability over time of the suspension resulting from the dispersion of the microbeads in the viscous polysaccharide solution. This screening study enabled to select alginate solution (4% *w/V*) with 30% *w/*w of microbeads as the best performing formulation, as this composition could be stored within syringes for 10 days maintaining the particles homogeneously distributed within the alginate medium (Figure 9A). The choice of alginate as a dispersant agent is also supported by literature studies: for example, Alves Cardoso *et al.* (2014) and Oliveira *et al.* (2008) reported the use of alginate for the preparation of an injectable, osteoconductive material based on HAp or calcium phosphate.

In order to assess the injectability of this formulation, the force required to extrude it through a syringe with a 2-mm nozzle diameter was tested by means of a universal testing machine. This diameter nozzle is in the typical range for cannulas used for bone cement injections (Tadier *et al.*, 2014). The results of the mechanical tests are reported in Figure 9B (blue line).

The data showed that it was possible to push the syringe plunger for the whole length of the syringe (50 mm) without stacking the particles or blocking the nozzle with an average compression load of 17 N (± 5 N), thus achieving a 100% extrusion of the paste. These values are in line with injectable materials developed by other authors (Perut *et al.*, 2011; Sohrabi *et al.*, 2013, 2014; Tadier *et al.*, 2014) and highlight the capability of this bone filler to be injected in a surgical procedure.

Another important feature of the formulation here-proposed is that during the storage and the extrusion of the formulation, no phase-separation phenomena of the microbeads from the liquid phase was observed. Phase separation is a critical issue for the injectable fillers as it may negatively affect the homogeneity and injectability of the materials (Tadier *et al.*, 2014).

In order to evaluate the morphology of the particles in the dispersion medium, a SEM investigation has been performed after withdrawing the microbeads from the alginate solution (Figure 10): the images showed that the particles displayed a smoother surface than the native microbeads. This could be ascribed to the adsorption of some alginate from the solution onto the microbeads surface.

In addition to the results obtained using alginate as dispersing agent, the possibility to add another polysaccharide to the solution has been explored with the aim to implement the bioactive properties of the injectable paste. To this end, hyaluronan has been selected as the additional solution component, given its healing capability and lubricating properties (Dicker

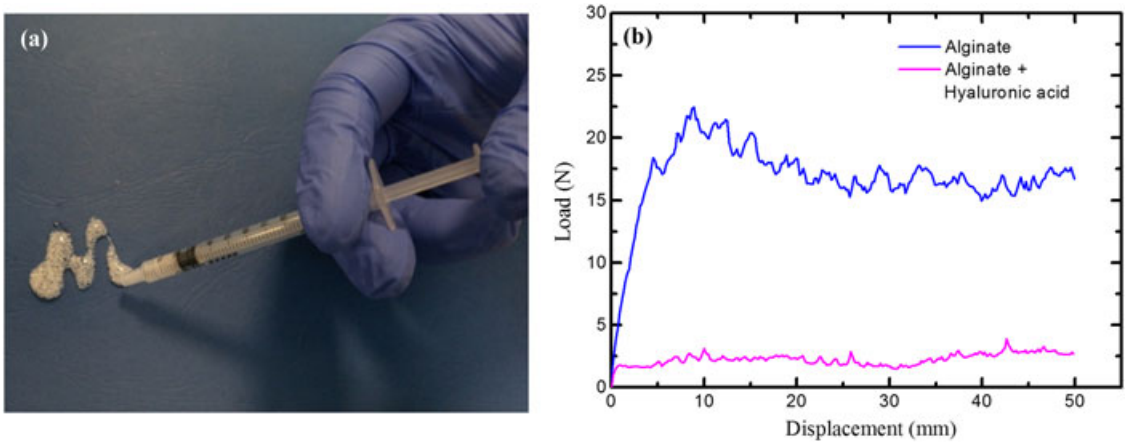

Figure 9. Injectability of MB microbeads dispersed in polysaccharide solutions. (A) Image of the syringe employed to extrude the injectable pastes. (B) Load-displacement (representative) curves recorded by compressing the plunger to extrude the paste out of the syringe. Blue line: 4% (*w/V*) alginate with 30% (*w/*w) MB microbeads

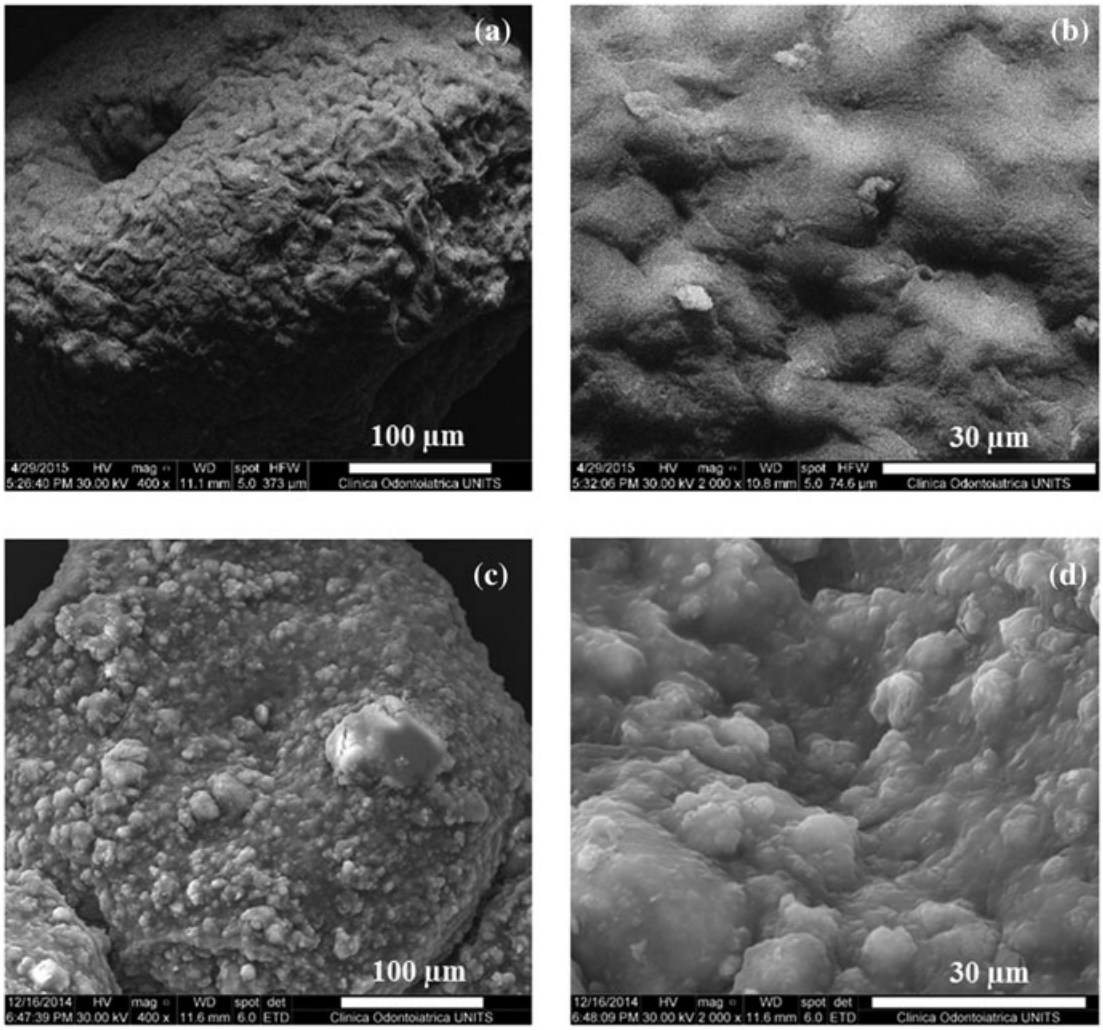

Figure 10. Scanning electron microscope (SEM) micrographs of alginate-coated MB microbeads (A, B) and of native MB microbeads (C, D)

et al., 2014). A high MW (1.5×10^6) HA sample was chosen (HA150). A mixed alginate/HA150 solution was prepared in which the concentration of the two polysaccharides was 3% *w/V* and 1% *w/V*, respectively, thus providing the same polymer mass concentration as in the HA-free case (4% *w/V*). Microbeads were added at the same content as in the pure alginate condition (30% *w*/w), also in this case obtaining a homogeneous dispersion that was tested in terms of injectability. The mechanical tests revealed that the presence of HA led to a considerable decrease of the force required for the extrusion of the injectable filler, with an average compression load of 2 N (± 1 N) required for the plunger to push the paste out of the syringe (Figure 9B, magenta line). Moreover, as observed in the formulation with alginate 4% *w/V*, phase-separation phenomena were not observed during the extrusion.

This finding suggests that the addition of HA to the alginate-microbeads paste is able to lubricate the particles during the extrusion through the syringe, while implementing the bioactive properties of the injectable biomaterial.

3.7. Conclusions

Microbeads based on HAp, alginate, and Chitlac–nAg were developed and characterized for the preparation of injectable bone fillers. The dried microbeads displayed a rapid swelling in contact with SBFs and maintained their integrity for more than 30 days. The evaluation of silver leakage from the microbeads showed that the antibacterial metal is slowly released in saline solution, with less than 6% of silver released after 1 week. Antibacterial tests *in vitro* proved that the microbeads displayed bactericidal effects toward *S. aureus*, *P. aeruginosa* and *S. epidermidis*, and that they were also able to damage pre-formed bacterial biofilms. The microbeads did not exert any cytotoxic effect towards osteoblast-like cells. Upon suspension of the particles in alginate (or alginate/hyaluronic acid) solution, a homogenous and time-stable paste was obtained; mechanical tests enabled to quantify the extrusion forces from surgical syringes, pointing out the good injectability of the material.

Overall, this novel antibacterial bone filler appears as a promising material for the treatment of bone defects, in

particular when possible infections could compromise the bone-healing process. Moreover, the components used for the preparation of the material (Chitlac and HAp) could also provide the filler with osteoconductive properties. A detailed characterization of the injectable paste, in terms of material properties and *in vivo* behaviour, will be the subject of a forthcoming study.

Acknowledgement

The scientific support from the inter-university Center for Biomaterials and Regenerative Medicine, BIOMA-TS, is gratefully acknowledged. This work has been carried out within the Cluster IRMI, Italian Regenerative Medicine Infrastructure. Mister Mattia Norrito is thanked for her skillful assistance in the experimental part. Confocal images of the fluorescein-labelled polysaccharide layers reported in this paper were generated in the Microscopy Center of the University of Trieste at the Life Sciences Department, funded as detailed at www.units.it/confocal.

Conflicts of interest

The authors have declared that there is no conflict of interest.

References

Alves Cardoso D, van den Beucken JJJP, Both LLH, Bender J, Jansen JA, Leeuwenburgh SCG. 2014; Gelation and biocompatibility of injectable alginate-calcium phosphate gels for bone regeneration. *J Biomed Mater Res Part A* **102**(3): 808–817.

Bongio M, van den Beucken JJJP, Leeuwenburgh SCG, Jansen JA. 2015; Preclinical evaluation of injectable bone substitute materials. *J Tissue Eng Regen Med* **9**(3): 191–209.

Campoccia D, Montanaro L, Arciola CR. 2006; The significance of infection related to orthopedic devices and issues of antibiotic resistance. *Biomaterials* **27**(11): 2331–2339.

Campoccia D, Montanaro L, Speziale P, Arciola CR. 2010; Antibiotic-loaded biomaterials and the risks for the spread of antibiotic resistance following their prophylactic and therapeutic clinical use. *Biomaterials* **31**(25): 6363–6377.

Chambers BA, Afrooz ARMN, Bae S, Aich N, Katz L, Saleh NB, Kirisits MJ. 2014; Effects of chloride and ionic strength on physical morphology, dissolution, and bacterial toxicity of silver nanoparticles. *Environ Sci Technol* **48**(1): 761–769.

Dicker KT, Gurski LA, Pradhan-Bhatt S, Witt RL, Farach-Carson MC, Jia X. 2014; Hyaluronan: a simple polysaccharide with diverse biological functions. *Acta Biomater* **10**(4): 1558–1570.

Díez-Pascual AM, Díez-Vicente AL. 2015; Wound healing bionanocomposites based on castor oil polymeric films reinforced with chitosan-modified ZnO nanoparticles. *Biomacromolecules* **16**(9): 2631–2644.

Diolosá M, Donati I, Turco G, Cadenaro M, Di Lenarda R, Breschi L, Paoletti S. 2014; Use of methacrylate-modified chitosan to increase the durability of dentine bonding systems. *Biomacromolecules* **15**(12): 4606–4613.

von Doernberg MCC, von Rechenberg B, Bohner M, Grünenfelder S, van Lenthe GH, Müller R, Gasser B, Mathys R, Baroud G, Auer J. 2006; In vivo behavior of calcium phosphate scaffolds with four different pore sizes. *Biomaterials* **27**(30): 5186–5198.

Donati I, Stredanska S, Silvestrini G, Vetere A, Marcon P, Marsich E, Mozetic P, Gamini A, Paoletti S, Vittur F. 2005; The aggregation of pig articular chondrocyte and synthesis of extracellular matrix by a lactose-modified chitosan. *Biomaterials* **26**: 987–998.

Gervaso F, Padmanabhan SK, Scalera F, Sannino A, Licciulli A. 2016; Mechanical stability of highly porous hydroxyapatite scaffolds during different stages of in vitro studies. *Mater Lett* **185**: 239–242.

Ghanaati S, Barbeck M, Hilbig U, Hoffmann C, Unger RE, Sader RA, Peters F, Kirkpatrick CJ. 2011; An injectable bone substitute composed of beta-tricalcium phosphate granules, methylcellulose and hyaluronic acid inhibits connective tissue influx into its implantation bed in vivo. *Acta Biomater* **7**(11): 4018–4028.

Gottenbos B, van der Mei HC, Busscher HJ. 2000; Initial adhesion and surface growth of *Staphylococcus epidermidis* and Pseudomonas aeruginosa on biomedical polymers. *J Biomed Mater Res* **50**(2): 208–214.

Goudouri OM, Kontonasaki E, Lohbauer U, Boccaccini AR. 2014; Antibacterial properties of metal and metalloid ions in chronic periodontitis and peri-implantitis therapy. *Acta Biomater* **10**(8): 3795–3810.

Gristina AG. 1987; Biomaterial-centered infection: microbial adhesion versus tissue integration. *Science* **237**(4822): 1588–1595.

Grynpas MD, Pilliar RM, Kandel RA, Renlund R, Filiaggi M, Dumitriu M. 2002; Porous calcium polyphosphate scaffolds for bone substitute applications in vivo studies. *Biomaterials* **23**(9): 2063–2070.

Guarino V, Caputo T, Altobelli R, Ambrosio L. 2015; Degradation properties and metabolic acrivity of alginate and chitosan polyelectrolytes for drug delivery and tissue engineering applications. *AIMS Mater Sci* **2**(4): 497–502.

ISO 10993-5 Standard. 1999; Biological Evaluation of Medical Devices – Part 5: Tests for In Vitro Cytotoxicity, ISO 10993-5. International Organization for Standardization: Geneva, Switzerland.

Kilgus DJ, Howe DJ, Strang A. 2002; Results of periprosthetic hip and knee infections caused by resistant bacteria. *Clin Orthop Relat Res* **404**: 116–124.

Kneser U, Schaefer DJ, Polykandriotis E, Horch RE. 2006; Tissue engineering of bone: the reconstructive surgeon's point of view. *J Cell Mol Med* **10**(1): 7–19.

Kokubo T, Kushitani H, Sakka S, Kitsugi T, Yamamuro T. 1990; Solutions able to reproduce in vivo surface-structure changes in bioactive glass-ceramic A-W^{3}. *J Biomed Mater Res Part A* **24**: 721–734.

Lara H, Garza-Trevino E, Ixtepan-Turrent L, Singh D. 2011; Silver nanoparticles are broad-spectrum bactericidal and virucidal compounds. *J Nanobiotechnol* **9**(1): 30.

Lee KY, Mooney DJ. 2012; Alginate: properties and biomedical applications. *Prog Polym Sci* **37**(1): 106–126.

Leid JG, Willson CJ, Shirtliff ME, Hassett DJ, Parsek MR, Jeffers AK. 2005; The exopolysaccharide alginate protects Pseudomonas aeruginosa biofilm bacreria from IFN-gamma-mediated macrophage killing. *J Immunol* **175**(11): 7512–7518.

Lewis G. 2011; Viscoelastic properties of injectable bone cements for orthopaedic applications: State-of-the-art review. *J Biomed Mater Res Part B* **98B**(1): 171–191.

Marsich E, Bellomo F, Turco G, Travan A, Donati I, Paoletti S. 2013a; Nano-composite scaffolds for bone tissue engineering containing silver nanoparticles: preparation, characterization and biological properties. *J Mater Sci Mater Med* **24**(7): 1799–1807.

Marsich E, Borgogna M, Donati I, Mozetic P, Strand BL, Salvador SG, Vittur F, Paoletti S. 2008; Alginate/lactose-modified chitosan hydrogels: a bioactive biomaterial for chondrocyte encapsulation. *J Biomed Mater Res Part A* **84A**(2): 364–376.

Marsich E, Travan A, Donati I, Turco G, Kulkova J, Moritz N, Aro HT, Crosera M, Paoletti S. 2013b; Biological responses of silver-coated thermosets: an in vitro and in vivo study. *Acta Biomater* **9**(2): 5088–5099.

Mauffrey C, Barlow BT, Smith W. 2015; Management of segmental bone defects. *JAOSS* **23**(3): 143–153.

Moran E, Byren I, Atkins BL. 2010; The diagnosis and management of prosthetic joint infections. *J Antimicrob Chemother* **65**(Suppl 3): iii45–iii54.

Morch YA, Donati I, Strand BL, Skjak-Braek G. 2006; Effect of Ca^{2+}, Ba^{2+}, and Sr^{2+} on alginate microbeads. *Biomacromolecules* **7**(5): 1471–1480.

Morones-Ramirez JR, Winkler JA, Spina CS, Collins JJ. 2013; Silver enhances antibiotic activity against gram-negative bacteria. *Sci Transl Med* **5**(190): 190ra81.

Nejadnik MR, Yang X, Bongio M, Alghamdi HS, van den Beucken JJJP, Huysmans MC, Jansen JA, Hilborn J, Ossipov D, Leeuwenburgh SCG. 2014; Self-healing hybrid nanocomposites consisting of bisphosphonated hyaluronan and calcium phosphate nanoparticles. *Biomaterials* **35**(25): 6918–6929.

Nganga S, Travan A, Marsich E, Donati I, Söderling E, Moritz N, Paoletti S, Vallittu P. 2013; In vitro antimicrobial properties of silver-polysaccharide coatings on porous fiber-reinforced composites for bone implants. *J Mater Sci Mater Med* **24**(12): 2775–2785.

Norowski PA, Bumgardner JD. 2009; Biomaterial and antibiotic strategies for peri-implantitis: a review. *J Biomed Mater Res Part B* **88B**(2): 530–543.

Oliveira SM, Barrias CC, Almeida IF, Costa PC, Ferreira MR, Bahia MF, Barbosa MA. 2008; Injectability of a bone filler system based on hydroxyapatite microspheres and a vehicle with in situ gel-forming ability. *J Biomed Mater Res Part B* **87**(1): 49–58.

Page JM, Harmata AJ, Guelcher SA. 2013; Design and development of reactive injectable and settable polymeric biomaterials. *J Biomed Mater Res Part A* **101**(12): 3630–3645.

Parvizi J, Azzam K, Ghanem E, Austin MS, Rothman RH. 2009; Periprosthetic infection due to resistant Staphylococci: serious problems on the horizon. *Clin Orthop Relat Res* **467**(7): 1732–1739.

Perut F, Montufar EB, Ciapetti G, Santin M, Salvage J, Traykova T, Planell JA, Ginebra MP, Baldini N. 2011; Novel soybean/gelatine-based bioactive and injectable hydroxyapatite foam: material properties and cell response. *Acta Biomater* **7**(4): 1780–1787.

Porrelli D, Travan A, Turco G, Marsich E, Borgogna M, Paoletti S, Donati I. 2015; Alginate-hydroxyapatite bone scaffolds with isotropic or anisotropic pore structure: material properties and biological behavior. *Macromol Mater Eng* **300**(10): 989–1000.

Reithofer MR, Lakshmanan A, Ping ATK, Chin JM, Hauser CAE. 2014; In situ synthesis of size-controlled, stable silver nanoparticles within ultrashort peptide hydrogels and their anti-bacterial properties. *Biomaterials* **35**(26): 7535–7542.

Sohrabi M, Hesaraki S, Kazemzadeh A. 2014; Injectable bioactive glass/polysaccharide polymers nanocomposites for bone sostitution. *Key Eng Mater* **614**: 41–46.

Sohrabi M, Hesaraki S, Kazemzadeh A, Alizadeh M. 2013; Development of injectable biocomposites from hyaluronic acid and bioactive glass nano-particles obtained from different sol-gel routes. *Mater Sci Eng C* **33**(7): 3730–3744.

Stojkovska J, Kostic D, Jovanovic Z, Vukasinovic Sekulic M, Miskovic Stankovic V, Obradovic B. 2014; A comprehensive approach to in vitro functional evaluation of Ag/alginate nanocomposite hydrogels. *Carbohydr Polym* **111**: 305–314.

Suzuki K, Anada T, Miyazaki T, Miyatake N, Honda Y, Kishimoto KN, Hosaka M, Imaizumi H, Itoi E, Suzuki O. 2014; Effect of addition of hyaluronic acids on the

osteoconductivity and biodegradability of synthetic octacalcium phosphate. *Acta Biomater* **10**(1): 531–543.

Tadier S, Galea L, Charbonnier B, Baroud G, Bohner M. 2014; Phase and size separations occurring during the injection of model pastes composed of b-tricalcium phosphate powder, glass beads and aqueous solutions. *Acta Biomater* **10**(5): 2259–2268.

Taglietti A, Arciola CR, D'Agostino A *et al*. 2014; Antibiofilm activity of a monolayer of silver nanoparticles anchored to an amino-silanized glass surface. *Biomaterials* **35**(6): 1779–1788.

Tan R, Feng Q, She Z, Wang M, Jin H, Li J, Yu X. 2010; In vitro and in vivo degradation of an injectable bone repair composite. *Polym Degrad Stab* **95**(9): 1736–1742.

Toms AD, Davidson D, Masri BA, Duncan CP. 2006; The management of peri-prosthetic infection in total joint arthroplasty. *J Bone Joint Surg Br* **88-B**(2): 149–155.

Travan A, Marsich E, Donati I, Foulc MP, Moritz N, Aro HT, Paoletti S. 2012; Polysaccharide-coated thermosets for orthopedic applications: from material characterization to in vivo tests. *Biomacromolecules* **13**(5): 1564–1572.

Travan A, Pelillo C, Donati I, Marsich E, Benincasa M, Scarpa T, Semeraro S, Turco G, Gennaro R, Paoletti S. 2009; Non-cytotoxic silver nanoparticle-polysaccharide nanocomposites with antimicrobial activity. *Biomacromolecules* **10**(6): 1429–1435.

Turco G, Marsich E, Bellomo F, Semeraro S, Donati I, Brun F, Grandolfo M, Accardo A, Paoletti S. 2009; Alginate/hydroxyapatite biocomposite for bone ingrowth: a trabecular structure with high and isotropic connectivity. *Biomacromolecules* **10**(6): 1575–1583.

Urist MR. 1965; Bone: formation by autoinduction. *Science* **150**(3698): 893–899.

Vold IMN, Kristiansen KA, Christensen BE. 2006; A study of the chain stiffness and extension of alginates, in vitro epimerized alginates, and periodate-oxidized alginates using size-exclusion chromatography combined with light scattering and viscosity detectors. *Biomacromolecules* **7**(7): 2136–2146.

Wei W, Abdullayev E, Hollister A, Mills D, Lvov YM. 2012; Clay nanotube/poly(methyl methacrylate) bone cement composites with sustained antibiotic release. *Macromol Mater Eng* **297**(7): 645–653.

Yalpani M, Hall LD. 1984; Some chemical and analytical aspects of polysaccharide modifications. Formation of branched-chain, soluble chitosan derivatives. *Macromolecules* **17**(3): 272–281.